

Multidecadal Changes of Upper-Ocean Thermal Conditions in the Tropical Northwest Pacific Ocean versus South China Sea during 1960–2015

TZU-LING CHIANG

Department of Earth Sciences, National Taiwan Normal University, Taipei, Taiwan

YI-CHIA HSIN

Research Center for Environmental Changes, Academia Sinica, Taipei, Taiwan

CHAU-RON WU

Department of Earth Sciences, National Taiwan Normal University, Taipei, Taiwan

(Manuscript received 9 June 2017, in final form 13 February 2018)

ABSTRACT

By analyzing the upper-ocean properties of observation-based hydrographic data and validated oceanic reanalysis products, this study presents multidecadal changes of oceanic surface and subsurface thermal conditions in the tropical northwest Pacific Ocean (TNWP) and South China Sea (SCS) during 1960–2015. The analysis reveals that a transition of a 30-yr trend took place in 1980s during the analyzed period for both the surface and subsurface environment. Generally, the warming trend of sea surface temperature (SST) in the TNWP has a similar multidecadal change to that in the SCS. However, a huge accumulating rate of upper-ocean heat content above the 26°C isotherm (UOHC26) showed up in the TNWP (about 3 times compared to that in the SCS) in the last 30 years. In the TNWP, the southward shift of the North Equatorial Current on the multidecadal time scale induces the vertical displacement of isotherms, leading to a strong subsurface warming around the top of the thermocline. Secondly, the Pacific decadal oscillation (PDO)-related SST regulates the thermal structure in the mixed layer. The multidecadal UOHC26 in the SCS is mainly attributed to the PDO-related SST and further modulated by the isothermal variability caused by the change of basin-scale SCS circulation.

1. Introduction

Upper-ocean thermal conditions play an important role in regulating the climate on a variety of time scales. For example, on time scales of hundreds to thousands of years, changes of surface temperature make a significant influence on the stability of thermohaline circulation (e.g., [Stocker and Schmittner 1997](#)). On interannual time scales, the El Niño–Southern Oscillation (ENSO) has been believed to be tied to the thermal structure in the equatorial ocean (e.g., [Jin 1997](#); [Wallace et al. 1998](#)). On shorter time scales (less than weeks), both sea surface temperature (SST) and upper-ocean thermal structure have been demonstrated to exert great impacts on the intensity of tropical cyclones (TCs) (e.g., [Price 1981](#); [Emanuel 1999](#); [Chan and Liu 2004](#); [Pun et al. 2007](#);

[Wu et al. 2007](#); [Lin et al. 2008](#); [Goni et al. 2009](#); [Chiang et al. 2011](#)).

Ocean temperature is influenced by many factors, such as solar radiation, winds, and ocean currents. These factors may exert their impacts on different aspects. For instance, solar radiation results in the diurnal and annual cycles of SST on a larger spatial scale. Winds impose momentum to the ocean and cause heat exchanges between the surface and subsurface layer. Ocean currents transmit heat both horizontally and vertically. The combined effect of winds and ocean currents form the zonal distribution of basin-scale SST. These complicated processes cause oceanic thermal conditions to be varied on various time scales from hours to thousands of years.

With time scales longer than decades, the warming of ocean temperature averaged over the globe has been proposed based on hydrographic observations and model simulations, and mainly ascribed to the global warming that is induced by the increase of atmospheric

Corresponding author: Dr. Chau-Ron Wu, cwu@ntnu.edu.tw

DOI: 10.1175/JCLI-D-17-0394.1

© 2018 American Meteorological Society. For information regarding reuse of this content and general copyright information, consult the [AMS Copyright Policy](#) (www.ametsoc.org/PUBSReuseLicenses).

CO₂ concentration (Trenberth et al. 2007). However, the warming in SST is highly inhomogeneous in space despite the nearly uniform increasing atmospheric CO₂ concentration (Belkin 2009; Wu et al. 2012). Besides, recent studies have demonstrated that the warming trend at the sea surface differs from that in the subsurface ocean (e.g., Huang et al. 2015; Zheng et al. 2015). That is, inconsistent warming in the ocean takes place not only horizontally but also vertically. This fact triggers us to explore the long-term changes in a regional ocean.

The focus of the present study is on the multidecadal changes of surface and subsurface thermal conditions in the northwest Pacific Ocean (NWP), which is one of the most active areas for TCs (Peduzzi et al. 2012), including the tropical northwest Pacific Ocean (TNWP; 5°–25°N, 121°–170°E) and South China Sea (SCS; 5°–25°N, 99°–121°E). Separated by the East and Southeast Asia island arcs, oceanic characteristics on the two sides of Luzon Strait are quite different (e.g., Chen and Huang 1996). Hence, upper-ocean thermal conditions are not alike between the TNWP and SCS. For example, Mei et al. (2015) proposed that mixed layer depth in the SCS is shallower but with stronger stratification in comparison with that in the TNWP.

Figure 1 demonstrates distinct climatological temperature patterns between the TNWP and SCS. As revealed in the temperature distributions at 0 and 50 m (Figs. 1a,b), an obvious discrepancy is found in that the horizontal gradients are northward in the TNWP but northwestward in the SCS. In other words, the temperature above 50 m is warmer in the southern (southeastern) part of the TNWP (SCS). A similar temperature pattern at 100 m is observed in the SCS, whereas a significant difference is found in the TNWP in comparison with those at 0 and 50 m (Fig. 1c). Unlike the monotonic northward increase of temperature above 50 m, a thermal trough occurs at the depth of 100 m around 5°–10°N, located between the westward-flowing North Equatorial Current (NEC) and eastward-flowing North Equatorial Countercurrent (NECC). The averages of temperature and the depth of 26°C isotherm (D26) in the TNWP and SCS are further summarized in Table 1. The differences of average temperature between the two regions are 0.2°, 1.4°, and 4.1°C at the depths of 0, 50, and 100 m, respectively. In addition, the calculation of D26 at different latitude shows that the mean D26 is deeper in the TNWP (about 1.5–2.5 times) than in the SCS (Fig. 1d and Table 1). These results point to the high discrepancy of temperature distribution between the TNWP and SCS.

To date, changes of upper-ocean temperature on centennial (e.g., global warming; Bindoff et al. 2007;

Trenberth et al. 2007), interdecadal [e.g., Pacific decadal oscillation (PDO); Mantua et al. 1997; Newman et al. 2016], and interannual (e.g., ENSO; Jin 1997; Wallace et al. 1998) time scales have been extensively investigated, while study of changes of upper-ocean thermal conditions (including surface and subsurface) on multidecadal time scales in a basin is still rare, let alone two basins. Thus, this study aims to discuss the difference of multidecadal changes in upper-ocean thermal conditions between the TNWP and SCS during 1960–2015 by analyzing observation-based hydrographic data and oceanic reanalysis products. Physical processes leading to the multidecadal oceanic variability are also proposed in the study. The rest of the paper is structured as follows. Section 2 describes the data and quantities utilized in this study, and section 3 briefly evaluates several oceanic reanalysis products, and the most suitable product is applied for this study. The multidecadal changes and possible mechanism of oceanic surface and subsurface thermal conditions in the TNWP and SCS are explored in detail in section 4. We also identified that ocean circulation variability plays a very important part in causing temperature to be warmed up or cooled down in the subsurface ocean. Finally, conclusions are given in section 5.

2. Data and quantities

Two observation-based hydrographic datasets are used in this study, climatological monthly temperature profile and monthly SST. The climatological monthly temperature data of the *World Ocean Atlas 2013* version 2 (*WOA13v2*; Locarnini et al. 2013) are provided by the Ocean Climate Laboratory/National Centers for Environmental Information/National Oceanic and Atmospheric Administration (<https://www.nodc.noaa.gov/about/oceanclimate.html>). The *WOA13v2* is a set of objectively analyzed ($1^\circ \times 1^\circ$) climatological fields of in situ temperature, salinity, dissolved oxygen, and nutrients at a new standard depth levels of 101 (for comparison, 33 standard levels were used in the previous *World Ocean Atlas* datasets) for the World Ocean. The long-term mean temperature in *WOA13v2* was computed for a time span of six decades (1955–2012), whereas data spanning only five decades were adopted in the older *WOA* datasets.

The monthly SST data adopted in this study are from the Hadley Centre Sea Ice and Sea Surface Temperature dataset (HadISST; Rayner et al. 2003), which is provided by the Hadley Centre/Met Office (<http://www.metoffice.gov.uk/hadobs/>). The HadISST dataset is a unique combination of monthly globally complete fields of SST and sea ice concentration on a $1^\circ \times 1^\circ$ grid

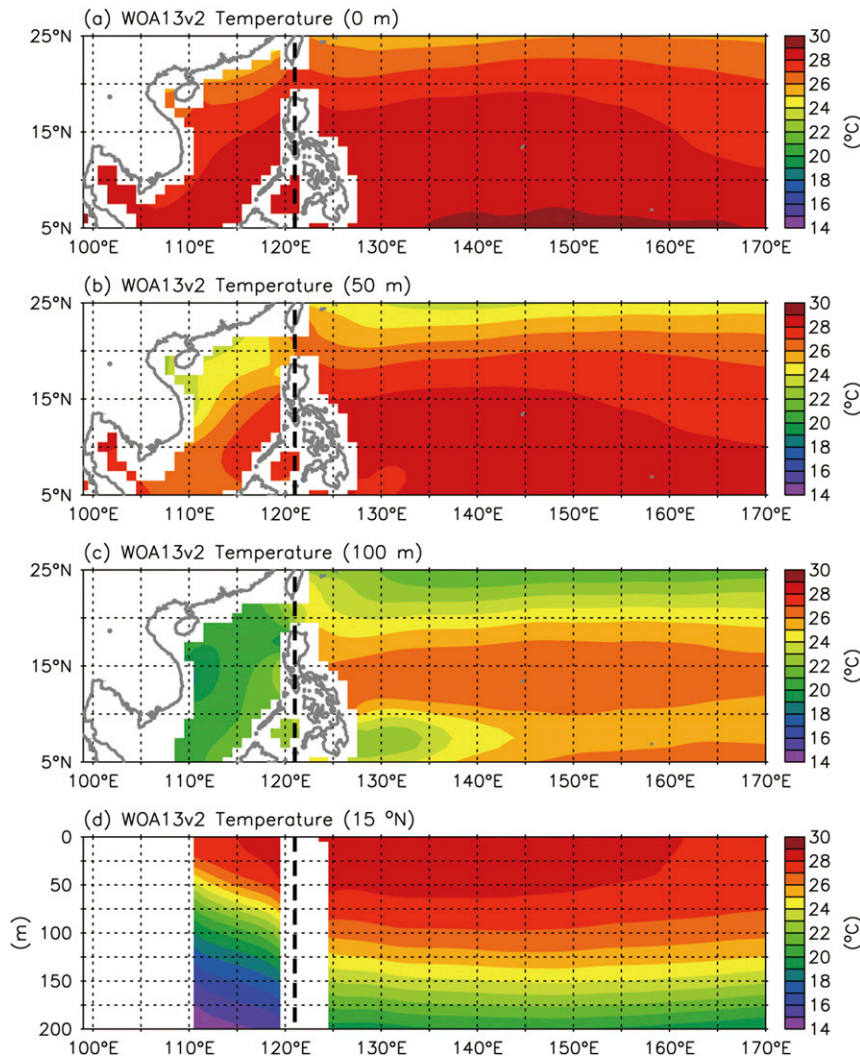


FIG. 1. Mean *WOA13v2* temperature distributions at (a) 0, (b) 50, and (c) 100 m, and along (d) 15°N. Thick dashed line denotes the latitude of 121°E.

from 1870 to date. In combined use of SST from the Met Office Marine Data Bank (MDB; 1982 to date) and Comprehensive Ocean Atmosphere Dataset (COADS; 1871–1995), the temperature in HadISST is reconstructed by using a two-stage reduced-space optimal interpolation procedure, followed by superposition of quality-improved gridded observations onto the reconstructions to restore local detail.

Oceanic reanalysis products assimilated with observations could provide a reliable and complete data continuous in both time and space, although they are always limited by the coarse spatial resolution of ~ 100 km and temporal interval of one month. Temperature profiles in oceanic reanalysis products are still able to provide us a good chance to investigate the spatiotemporal basin-scale variability of both surface

and subsurface thermal conditions on multidecadal time scales. There are more than 10 oceanic reanalysis products available since 1960 (Hsin 2016). Only three oceanic reanalysis products cover periods up to 2014. One is $1^\circ \times 1^\circ$, the European Centre for Medium-Range

TABLE 1. Mean temperature ($^\circ\text{C}$) at different depth and D26 (m) at different latitude of the *WOA13v2* in the TNWP and SCS.

<i>WOA13v2</i>	TNWP	SCS
Temperature (0 m)	28.0	27.8
Temperature (50 m)	27.4	26.0
Temperature (100 m)	25.0	20.9
D26 (10°N)	92	57
D26 (15°N)	114	49
D26 (20°N)	70	40

Weather Forecasts (ECMWF) Ocean Reanalysis System 4 (ORAS4; <http://www.ecmwf.int/en/research/climate-reanalysis/ocean-reanalysis>; [Balmaseda et al. 2013](#)) from 1958 to 2015, another is $2^\circ \times 1^\circ$, the Predictive Ocean Atmosphere Model for Australia (POAMA) Ensemble Ocean Data Assimilation System (PEODAS; <http://poama.bom.gov.au>; [Yin et al. 2011](#)) from 1960 to 2014; and the third is the $1^\circ \times 1/3^\circ$ German contribution of the Estimating the Circulation and Climate of the Ocean project 2 (GECCO2; <https://icdc.cen.uni-hamburg.de/1/daten/reanalysis-ocean/gecco2.html>; [Köhl 2015](#)) from 1948 to 2014 distributed by the Integrated Climate Data Center/Center for Earth System Research and Sustainability. All oceanic reanalysis products are re-gridded onto 1° latitude–longitude grid for further analyses.

Quantities utilized in this study include the upper-ocean heat content. The upper-ocean heat content referred to 26°C (UOHC26) is the vertical integration of temperature anomalies above the isothermal surface of 26°C , and is derived by the formula $c_p \int_{z=D26}^{z=0} \rho(T - 26) dz$ ([Leipper and Volgenau 1972](#)), where c_p is specific heat, T is water temperature in $^\circ\text{C}$, ρ is seawater density, z is depth, and D26 is depth of the 26°C isotherm.

3. Brief evaluation of the oceanic reanalysis products

[Hsin \(2016\)](#) has compared mean spatial patterns of zonal velocity from the three oceanic reanalysis products with Argo drifter-derived data over 15°S – 20°N in the Pacific Ocean. Time series of monthly zonal velocity were also compared with the ADCPs (acoustic Doppler current profilers) and current meters observed at the TAO/TRITON (Tropical Atmosphere Ocean/Triangle Trans-Ocean Buoy Network) array. The comparison reveals that the three products can well reproduce the velocity field in the tropical Pacific (correlation coefficients are > 0.8 for the mean pattern and > 0.75 for temporal variation).

Furthermore, we have evaluated mean temperature and D26 from the three oceanic reanalysis products with the *WOA13v2* in the TNWP and SCS. In addition, temporal variations of D26 from the three products were also evaluated with gridded Argo data (<http://apdrc.soest.hawaii.edu/projects/argo/>). As revealed in [Fig. 2a](#), the observed D26 in the SCS is, on average, deeper in the southeast part, and that in the TNWP is deeper along the latitude of $\sim 15^\circ\text{N}$. In general, the spatial patterns of D26 in the three products are alike. Larger discrepancies are found in the PEODAS for the SCS and in the GECCO2 for the TNWP.

To further quantitatively compare mean D26 in the three reanalysis products with that in the *WOA13v2*, the pattern correlation analysis (i.e., correlation in the space domain) and root-mean-square error (RMSE) referred to in the *WOA13v2* are carried out for different regions of the TNWP and SCS ([Table 2](#)). By comparing pattern correlation coefficients and RMSEs among the three products, there is the worst correlation in GECCO2 for the TNWP and in PEODAS for the SCS. In terms of the RMSE, the largest value occurs in GECCO2 and PEODAS for the TNWP and SCS, respectively. This outcome indicates again that a larger discrepancy of the D26 pattern exists in GECCO2 (PEODAS) for the TNWP (SCS).

Another intercomparison is also performed for the depth-dependent mean temperature and latitude-dependent mean D26 in the TNWP and SCS ([Tables 1 and 3](#)). Generally, the values of temperature and D26 in the TNWP and SCS of ORAS4 are close to those derived from the *WOA13v2*, but the values of PEODAS (GECCO2) in the SCS (TNWP and SCS) have a greater difference from those in *WOA13v2*. The depth-dependent RMSEs of temperature referred to in the *WOA13v2* are calculated in [Fig. 3](#) to further compare the performance of temperature at different depth in the three oceanic products. In both the TNWP and SCS, the temperature in the ORAS4 deviates less from the observations, consistent with the above comparisons.

Although gridded Argo data do not cover the region in the SCS and the period before 2004, the gridded Argo data still provide some observational base for the comparison of temporal variation. The correlation coefficient of monthly D26 time series in the TNWP between the ORAS4, PEODAS, and GECCO2 and gridded Argo data is higher than 0.97, 0.97, and 0.95, respectively. Based on the above analyses, we can simply conclude that the ORAS4 is the most suitable oceanic reanalysis product to be used in this study.

4. Results and discussion

a. Multidecadal changes in oceanic surface conditions in the TNWP versus SCS

[Figure 4](#) shows the time series with a 5-yr moving average of HadISST SST anomalies (1960–2015) averaged in the TNWP and SCS. The SSTs in both the TNWP and SCS have warming tendencies in the period of 1960–2015, and their linear trends are $\sim 1^\circ\text{C} (100 \text{ yr})^{-1}$ and $\sim 1.5^\circ\text{C} (100 \text{ yr})^{-1}$ in the TNWP (red line in [Fig. 4a](#)) and SCS (orange line in [Fig. 4b](#)), respectively. Besides the whole analyzed period in 1960–2015, linear trends in the first 30 years (green lines in [Figs. 4a,b](#)) and

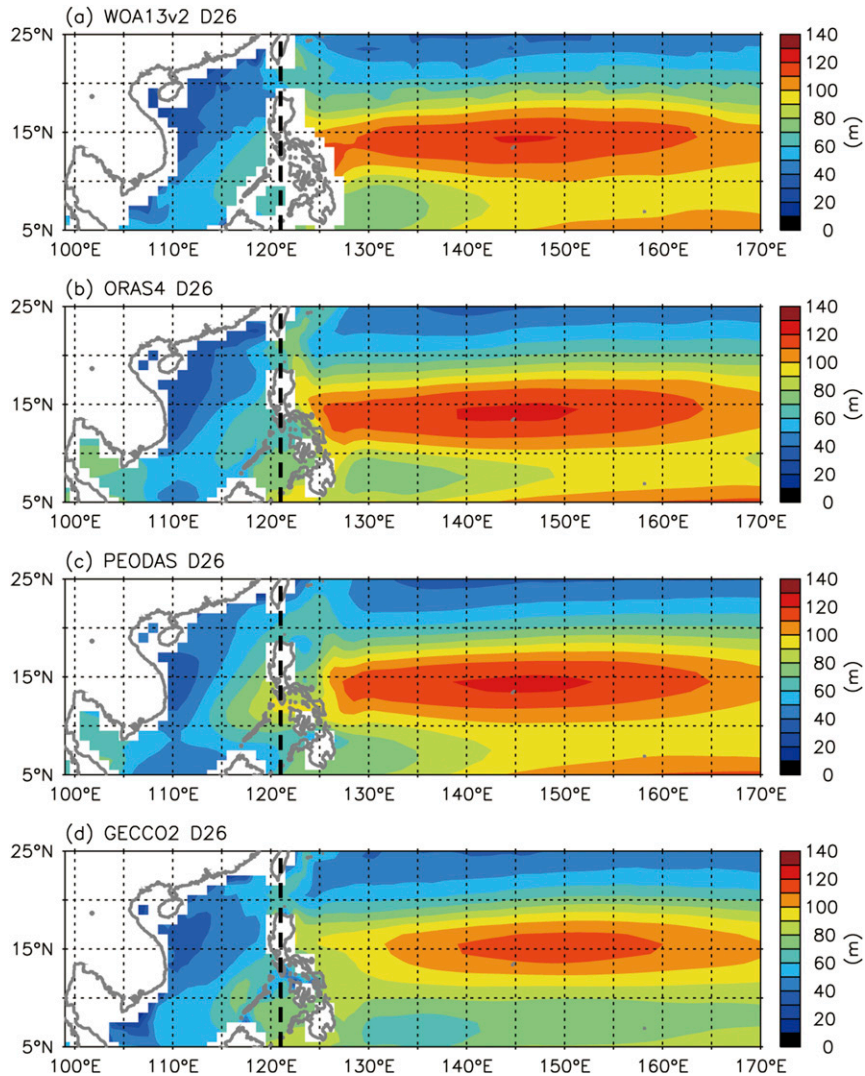


FIG. 2. Mean D26 distributions calculated from the (a) *WOA13v2* (1955–2012), (b) *ORAS4* (1960–2015), (c) *PEODAS* (1960–2014), and (d) *GECCO2* (1960–2014). Thick dashed line denotes the latitude of 121°E.

the last 30 years (blue lines in Figs. 4a,b) are also estimated to clarify whether a multidecadal change occurred in the past ~6 decades. The linear trends in the TNWP during 1960–89 and 1986–2015 are about 0.9° and $1.2^{\circ}\text{C} (100\text{yr})^{-1}$, whereas those in the SCS are 1.6° and $1.2^{\circ}\text{C} (100\text{yr})^{-1}$, respectively. The results show that linear trends of SST increased steadily with a slight change [0.3° – $0.4^{\circ}\text{C} (100\text{yr})^{-1}$] from the former three decades to the latter three decades in both the TNWP and SCS. It is noteworthy that a slight increase of warming rate in the latter 30 years happened in the TNWP, whereas the warming rate in the same duration flattened in the SCS.

As mentioned in the introduction, the warming rate at the sea surface varies spatially. During the entire analyzed period (Fig. 5a), there is a general warming

tendency with the highest value in the vicinity of Taiwan and smaller values (even cooling) to the east of $\sim 150^{\circ}\text{E}$. Similar spatial patterns are obtained as the period of the former three decades (1960–89) is adopted (Fig. 5b).

TABLE 2. Mean D26 pattern correlation analysis between three oceanic reanalysis products and *WOA13v2*, and RMSE of D26 (m) referred to the *WOA13v2* calculated from three oceanic reanalysis in the TNWP and SCS.

D26	Pattern correlation coefficient		RMSE	
	TNWP	SCS	TNWP	SCS
ORAS4 (1960–2015)	0.98	0.78	4.08	7.97
PEODAS (1960–2014)	0.99	0.70	4.33	10.62
GECCO2 (1960–2014)	0.92	0.83	11.43	7.67

TABLE 3. Mean temperature ($^{\circ}\text{C}$) at different depth and D26 (m) at different latitude of the ORAS4, PEODAS, and GECCO2 in the TNWP and SCS. Asterisks (*) indicate $T > \text{WOA13v2} \pm 0.5^{\circ}\text{C}$, $\text{D26} > \text{WOA13v2} \pm 5 \text{ m}$

	TNWP	ORAS4 (1960–2015)	PEODAS (1960–2014)	GECCO2 (1960–2014)
Temperature (0 m)		28.1	28.1	28.4
Temperature (50 m)		27.6	27.3	27.6
Temperature (100 m)		24.9	25.0	24.7
D26 (10°N)		89	90	78*
D26 (15°N)		115	113	105*
D26 (20°N)		73	72	72
	SCS	ORAS4 (1960–2015)	PEODAS (1960–2014)	GECCO2 (1960–2014)
Temperature (0 m)		27.8	27.8	28.1
Temperature (50 m)		26.4	26.0	26.4
Temperature (100 m)		21.3	22.1*	22.7*
D26 (10°N)		62	61	59
D26 (15°N)		50	57*	48
D26 (20°N)		42	50*	45

However, one can find that a stronger east–west contrast appears along $\sim 150^{\circ}\text{E}$; that is, a stronger warming (cooling) trend shows up to the west (east) of $\sim 150^{\circ}\text{E}$. A dramatic change took place in the recent three decades (Fig. 5c). Although the entire studied area warmed up

concurrently, the warming rate to the west of 150°E has been getting slower and the ocean to the east of 150°E changes from a cooling environment to a warming one. In the SCS, the multidecadal change of spatial distribution of SST anomaly simply represents that of the

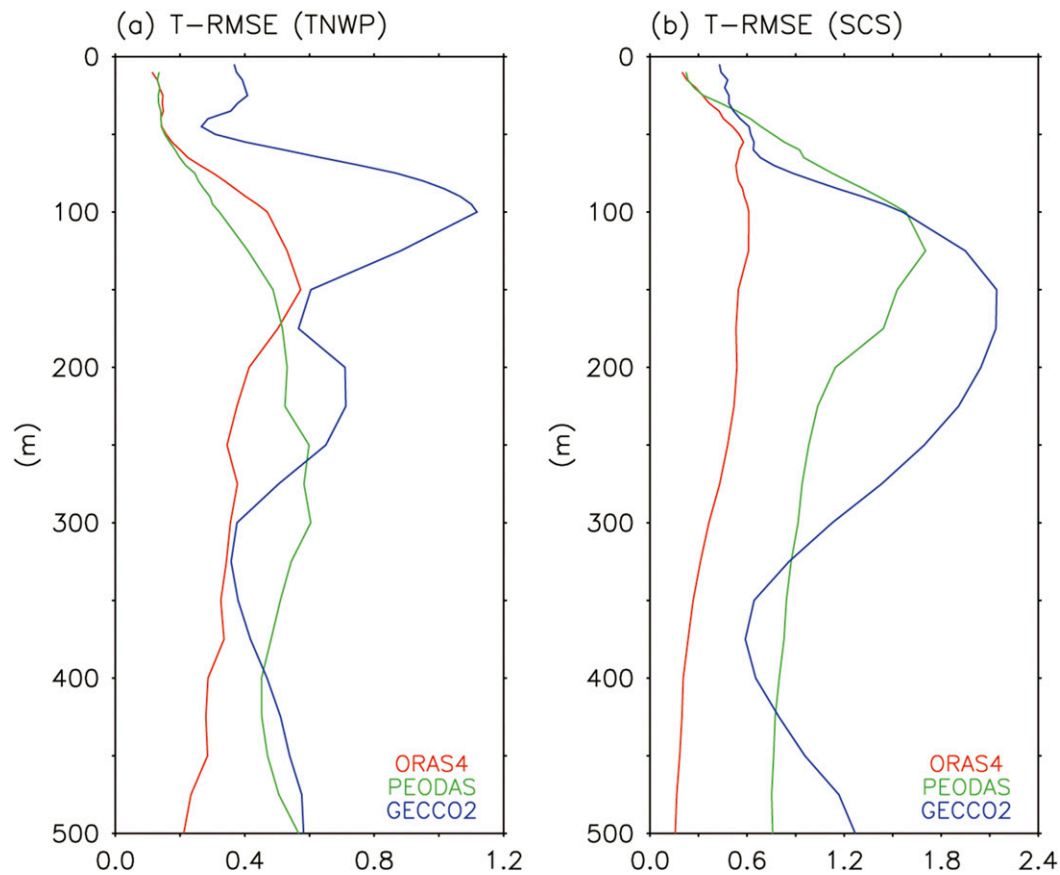


FIG. 3. RMSEs of temperature ($^{\circ}\text{C}$) referred to in the *WOA13v2* calculated from the ORAS4, PEODAS, and GECCO2 in the (a) TNWP and (b) SCS.

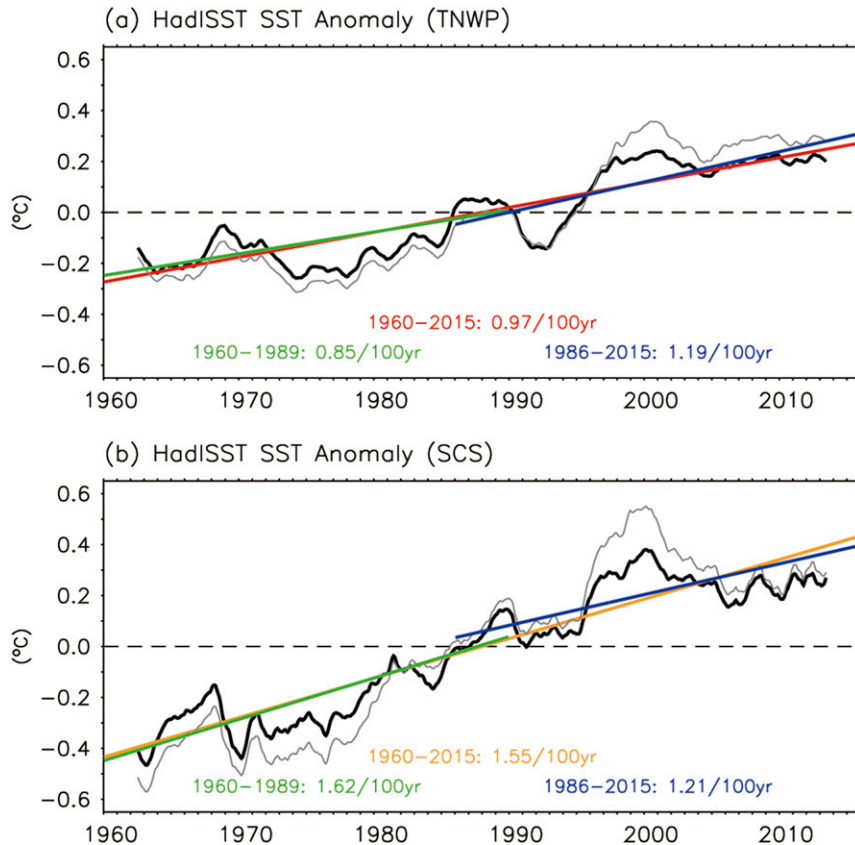


FIG. 4. Time series of HadISST SST anomaly with a 5-yr moving average in the (a) TNWP and (b) SCS. Red and orange lines denote the linear trend during 1960–2015. Green and blue lines indicate the linear trends during 1960–89 and 1986–2015, respectively. Black thin lines denote time series of the ORAS4 SST anomaly with a 5-yr moving average.

domain-averaged SST anomaly shown in Fig. 4b. However, the multidecadal change of SST anomaly in the TNWP exhibits a contrast between the two sides of $\sim 150^{\circ}\text{E}$, which results in a faster increasing rate of domain-averaged SST anomaly in the entire TNWP after the 1980s (Fig. 4a).

b. Multidecadal changes in subsurface conditions in the TNWP versus the SCS

Figure 6 depicts the 5-yr moving averaged time series of ORAS4 UOHC26 anomaly averaged spatially over the TNWP and SCS. During 1960–2015, the UOHC26s in the TNWP and SCS increased with a linear trend of $\sim 50 \text{ KJ cm}^{-2} (100 \text{ yr})^{-1}$ and $\sim 40 \text{ KJ cm}^{-2} (100 \text{ yr})^{-1}$, respectively. In 1960–89 (1986–2015), the linear trends of UOHC26 are about 31 (95) $\text{KJ cm}^{-2} (100 \text{ yr})^{-1}$ in the TNWP and 37 (34) $\text{KJ cm}^{-2} (100 \text{ yr})^{-1}$ in the SCS. This result indicates that the change of multidecadal trends from the former 30 years to the latter 30 years in the TNWP significantly differs from that in the SCS. The increase of UOHC26 in the SCS has been slowed down

in the latter three decades when more and more heat has been accumulated in the TNWP with a faster (~ 3 times greater) increasing rate.

Similarly, the spatial distribution of UOHC26 trend is further examined in Fig. 7. One can find that the tendency patterns of subsurface conditions are totally dissimilar to those of the surface conditions, especially in the TNWP. In the SCS, the trends of UOHC26 are about $0\text{--}40 \text{ KJ cm}^{-2} (100 \text{ yr})^{-1}$ regardless of analyzed period (including 1960–2015, 1960–89, and 1986–2015). In 1960–2015, the increasing rate of UOHC26 in the TNWP is, on average, greater than that in the SCS (Fig. 7a). More complicated multidecadal changes of spatial distribution of accumulating rate of heat content show up in the TNWP (Figs. 7b,c).

In the three decades between the 1960s and 1980s, a broad accumulated UOHC26 area was found to the west of $\sim 150^{\circ}\text{E}$ and scaled down to a smaller area in the northern part to the east of $\sim 150^{\circ}\text{E}$ (Fig. 7b). Besides, a significant releasing rate of heat content was observed in the southern part to the east of $\sim 150^{\circ}\text{E}$. In the three

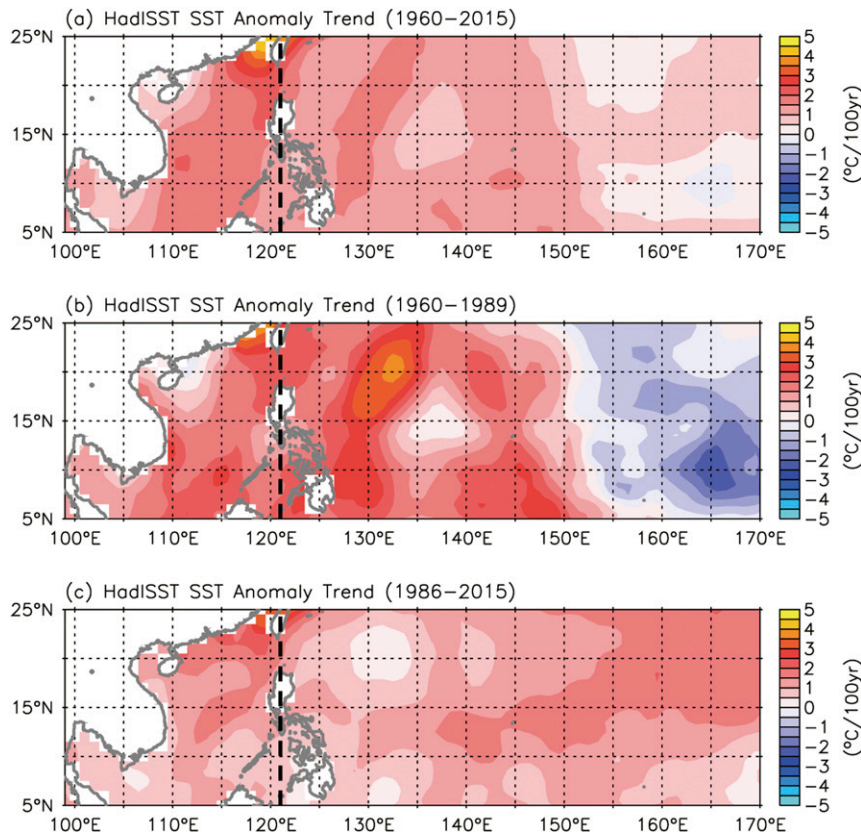


FIG. 5. Linear trends of the HadISST SST anomaly during (a) 1960–2015, (b) 1960–89, and (c) 1986–2015. Thick dashed line denotes the longitude of 121°E.

decades of 1986–2015, the UOHC26 in the TNWP accumulated faster to the south of 18°–20°N with the fastest accumulating rate [$>100 \text{ KJ cm}^{-2} (100 \text{ yr})^{-1}$] along the latitudes of 5°–18°N (Fig. 7c). To the north of 18°–20°N, an opposite multidecadal variation occurred; that is, the accumulating heat content became a releasing one, and vice versa. Another significant multidecadal change occurred in the southern part to the east of 150°E where the releasing heat content changed to be accumulative.

c. Transition period of multidecadal trends

The multidecadal trends of oceanic environment have been proposed in the previous two subsections. One of the questions is when the multidecadal trends transition. Analyses of moving trend with a time window of 30 years are carried out for the SST and UOHC26 (Fig. 8) to examine when the transition periods of trend took place for these two upper-ocean thermal conditions. As revealed in Fig. 8a, the 30-yr moving trend of the HadISST SST anomaly from 1960 to 2015 is positive in both the TNWP and SCS (red and orange lines), indicative of a continuous warming at the sea surface, but

the warming rate in the SCS is higher than that in the TNWP. One can find a trend transition of the warming rates occurring in the 1980s. Before the 1980s, the warming rate in the SCS and TNWP speeded up with a similar temporal evolution. This condition changed dramatically after the 1980s. The warming rate in the TNWP reduced slightly after the 1980s, whereas that in the SCS dropped quickly from 2.5° to $1.5^\circ \text{C} (100 \text{ yr})^{-1}$. The warming rates in the TNWP and SCS became close and had a similar changing tendency after the 1990s.

A similar transition period of trend appears in the UOHC26 field with different changing tendencies in the TNWP and SCS, and the heat content in upper oceans of the TNWP and SCS accumulated continuously in the entire analyzed period of ~ 6 decades (red and orange lines in Fig. 8b). In the SCS, the temporal evolution of the UOHC26 accumulating rate almost follows that of SST warming rate. In the TNWP, the accumulating rate of oceanic heat content varied in a small range of $15\text{--}30 \text{ KJ cm}^{-2} (100 \text{ yr})^{-1}$ in 1970s, suffered an abruptly rise to $80 \text{ KJ cm}^{-2} (100 \text{ yr})^{-1}$ in the 1980s, and kept a magnitude larger than $80 \text{ KJ cm}^{-2} (100 \text{ yr})^{-1}$ with a slight increase after the 1990s. The transition period (1980s) of

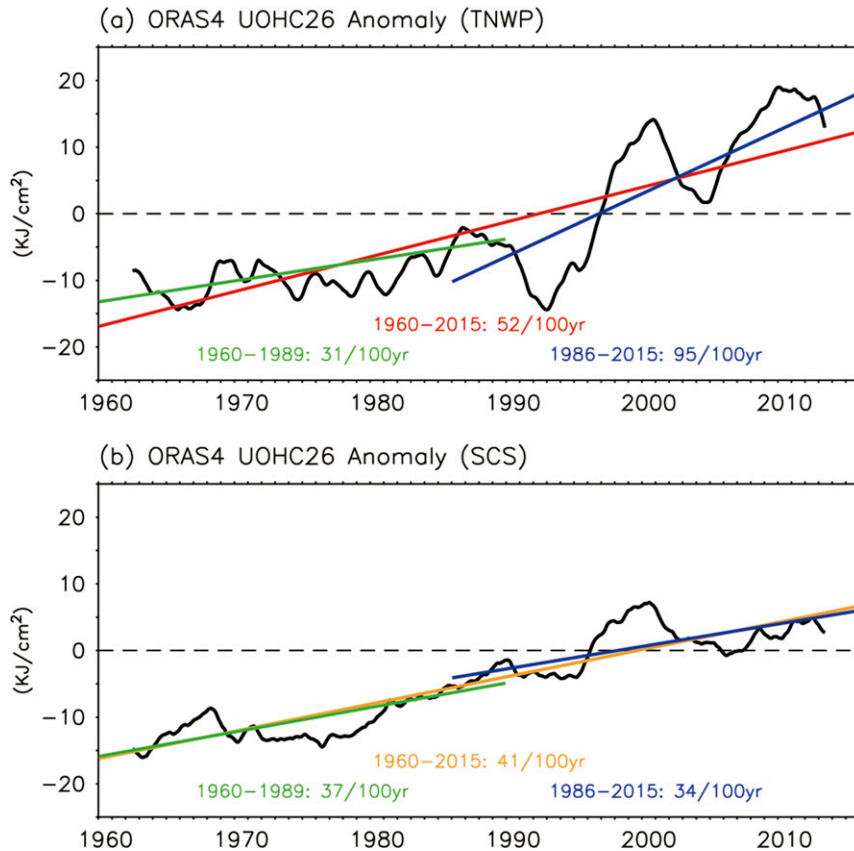


FIG. 6. Time series of the ORAS4 UOHC26 anomaly with a 5-yr moving average in the (a) TNWP and (b) SCS. Red and orange lines denote the linear trend during 1960–2015. Green and blue lines indicate the linear trends during 1960–89 and 1986–2015, respectively.

multidecadal trends in the SST and UOHC26 with a time window of 30 years (Fig. 8) could result from an abrupt change of SST and UOHC26 anomalies in the beginning of the 1990s (Figs. 4 and 6). This abrupt change has been proposed to be related to the regime shift of SST in the 1990s (Yu et al. 2012; Thompson et al. 2017).

One may notice that a large difference of multidecadal warming trends shows up between the areas west and east of $\sim 150^{\circ}\text{E}$ in the TNWP (hereafter TNWPw and TNWPe; Figs. 5 and 7). Therefore, it is necessary to further examine regional discrepancy in the TNWP. As shown in Fig. 8a, the trends of SST in the TNWPw and TNWPe transited in the same period as the TNWP and SCS, indicative of the robust transition period of the warming trend in the whole NWP. It is noteworthy that the TNWPw and TNWPe had a consistent evolution of warming rate with the TNWP after 1980s. Before the 1980s, the increased warming rate of SST in the TNWPw changed a little in the range of $1.5^{\circ}\text{--}2^{\circ}\text{C} (100\text{yr})^{-1}$, but the SST in the TNWPe suffered a huge transition from a cooling environment

to a warming one in the end of the 1970s. The evolutions of SST trends in the TNWPw and TNWPe are similar after 1980s.

As to the UOHC26 (Fig. 8b), a larger difference of the accumulating rate can be also found between TNWPw and TNWPe in the 1970s. The accumulating rate in the TNWPw reduced but that in the TNWPe remained nearly constant. After the early 1980s, the UOHC26 trends in the two regions had a consistent evolution with that in the whole TNWP. In sum, both the surface and subsurface ocean thermal conditions experienced multidecadal changes with a transition in the 1980s.

d. Possible mechanism

The PDO is considered to be the most important decadal climate variability in the Pacific Ocean. More and more studies (e.g., Qiu 2003; Han and Huang 2008; Wu 2013; Newman et al. 2016; Wu et al. 2016) have focused on discussing how PDO-related atmospheric variability results in the oceanic variations (e.g., SST, sea surface height, current intensity, and bifurcation latitude of current) in the North Pacific Ocean on time scales longer

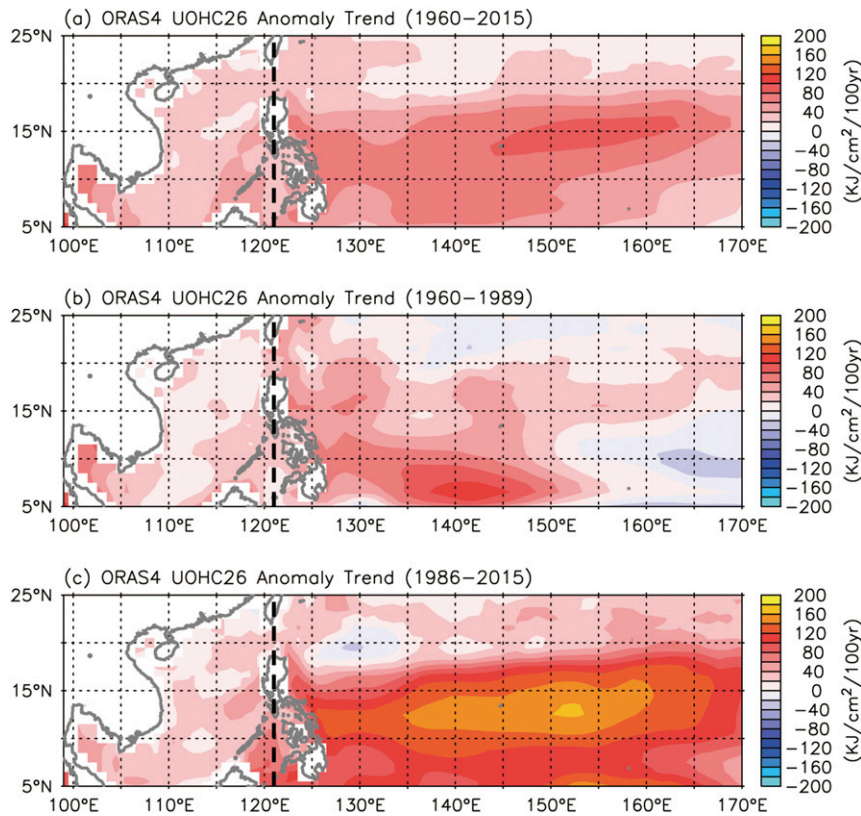


FIG. 7. Linear trends of the ORAS4 UOHC26 anomaly during (a) 1960–2015, (b) 1960–89, and (c) 1986–2015. Thick dashed line denotes the longitude of 121°E.

than a decade. The PDO, defined as the leading principal component of monthly SST anomalies in the North Pacific Ocean (Fig. 9a), is a climate phenomenon with an internal switch between warm phase (positive index) and cold phase (negative index) at a period of 20–30 years. Thus, the multidecadal changes of SST in the NWP could be connected with the PDO. Considering the temporal evolution and spatial pattern of the PDO (Figs. 9a,b), PDO-related SST anomalies contribute negative values in the TNWPe during the warm PDO phase.

During the 1960s to 1980s, the first three decades in the analyzed period, the 30-yr low-pass filtered (based on fast Fourier transform with a rectangular window of a 30-yr cutoff period) the PDO index increased and transitioned from the cold phase to the warm phase, supporting a cooling trend of SST in the TNWPe (east of 150°E), a warming trend in the SCS, and an unobvious trend in between (the TNWPw), shown in Figs. 5b and 8a. Furthermore, when the filtered PDO index had an opposite tendency with decreasing and shifting from a warm phase to a cold phase during the 1930s to 1960s, the spatial pattern of SST trend in the whole NWP area reversed (Fig. 9c). During the latter three decades in the

analyzed period, the filtered PDO index ran at a decreasing tendency from a large and positive value to a slightly negative one. This weaker change in the PDO resulted in a weaker contrast of trends between the west and east of 150°E compared with the events in the 1930s to 1960s (cf. Figs. 5c and 9c). In other words, the SST in the TNWPw presented a weaker warming tendency whereas that in the TNWPe had a stronger one (Fig. 5c). To sum up, the multidecadal change of SST in the NWP is ascribed to the basin-scale decadal oscillation in the Pacific Ocean.

According to the definition in section 2, the UOHC26 is the integrated effect of the temperature profile above the D26. As discussed in the previous sections, there are some similarities of multidecadal changes between the surface (SST) and subsurface (UOHC26) conditions. A transition period of trend in 1980s took place and there was an opposite multidecadal tendency between the west and east of ~150°E. Therefore, one may attempt to ascribe the multidecadal change of UOHC26 to the multidecadal change of SST. However, when comparing the spatial distributions of SST and UOHC26 trends in 1960–89 and 1986–2015, some obvious discrepancies are found. For example, in 1960–89, a more complicated

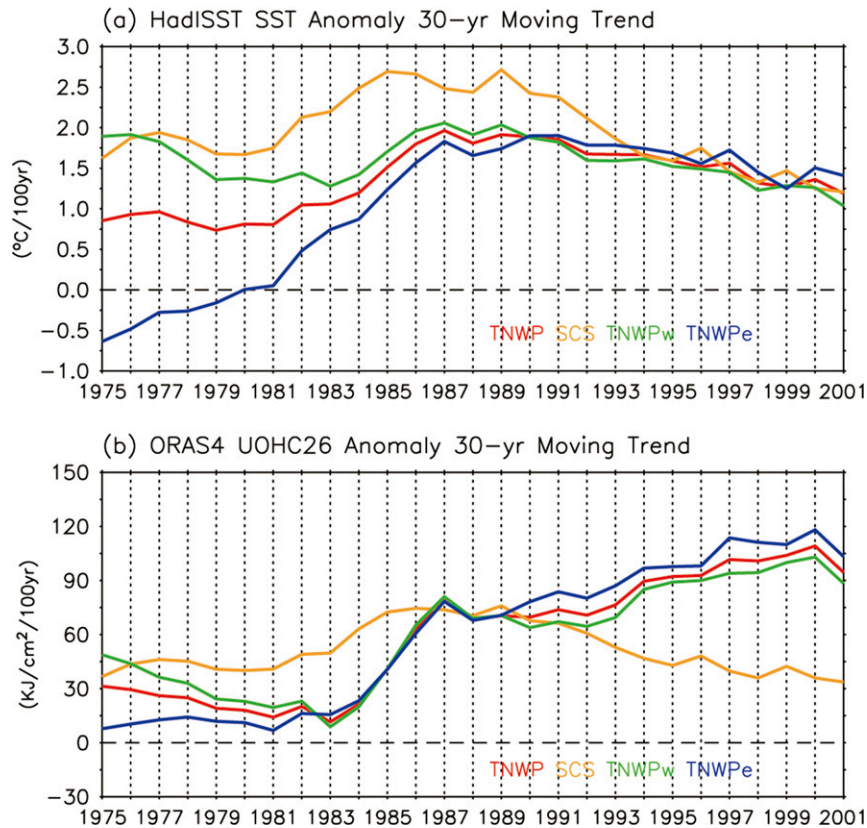


FIG. 8. Moving trends of the (a) HadISST SST anomaly and (b) ORAS4 UOHC26 anomaly in the TNWP, SCS, TNWPw, and TNWPe in 1960–2015 with a window of 30 yr. Labeled year on the x -axis denotes the center of each 30-yr window.

distribution was found in the UOHC26 than in the SST (cf. Figs. 5b and 7b). During 1986–2015, the UOHC26 trend was positive in most of the TNWP and SCS with very large values along the latitudes of 5° – 18° N in the TNWP, whereas the SST had a weaker warming rate in the entire studied area (cf. Figs. 5c and 7c). Thus, the outcome shows that the multidecadal change of SST is not sufficient to directly address the multidecadal change in the subsurface ocean.

As mentioned above, multidecadal trends in the UOHC26 are significantly different to the east and west of 150° E; therefore, multidecadal trends of UOHC26, D26, and temperature profiles averaged in 135° – 140° E (west of 150° E) and 160° – 165° E (east of 150° E) are adopted to clarify the processes resulting in the multidecadal change of upper-ocean heat content in the two regions (Figs. 10 and 11). To the west of 150° E (Fig. 10a), the multidecadal trends of UOHC26 in 1960–89 (red line) peaked at 5° – 7° N and dropped toward the north to negative values to the north of 21° N; those in 1986–2015 (blue line) had a maximal accumulating rate at 12° – 13° N and smaller ones to the north of $\sim 19^{\circ}$ N. Similar changes are found in the multidecadal trends of D26 for both

periods (Fig. 10c). To the east of 150° E (Fig. 10b), the UOHC26 in 1960–89 (red line) had smaller accumulating/releasing trends varying at a range of $-30 \sim 30 \text{ KJ cm}^{-2} (100 \text{ yr})^{-1}$ with a maximum at 16° – 17° N, whereas those in 1986–2015 (blue line) kept compatible accumulative trends as in the area west of 150° E (Fig. 10a). In comparison with the multidecadal trends of D26 (Fig. 10d), similar change is only found for the period of 1986–2015.

To clarify the changes of temperature profiles responsible for the multidecadal change of UOHC26, trends of depth-dependent temperature above D26 are depicted in Fig. 11 for the first half (black contour) and last half (green contour) of both three-decade periods (1960–1989 and 1986–2015). To the west of 150° E, warming occurred in the whole water column above D26 during both three-decade periods (shading in Figs. 11a,c). However, the temperature to the east of 150° E suffered a cooling trend in the surface layer with a warming trend below the $\sim 27.5^{\circ}\text{C}$ isotherm in 1960–89 (Fig. 11b) whereas that warmed up in the whole water column above the D26 in 1986–2015 (Fig. 11d).

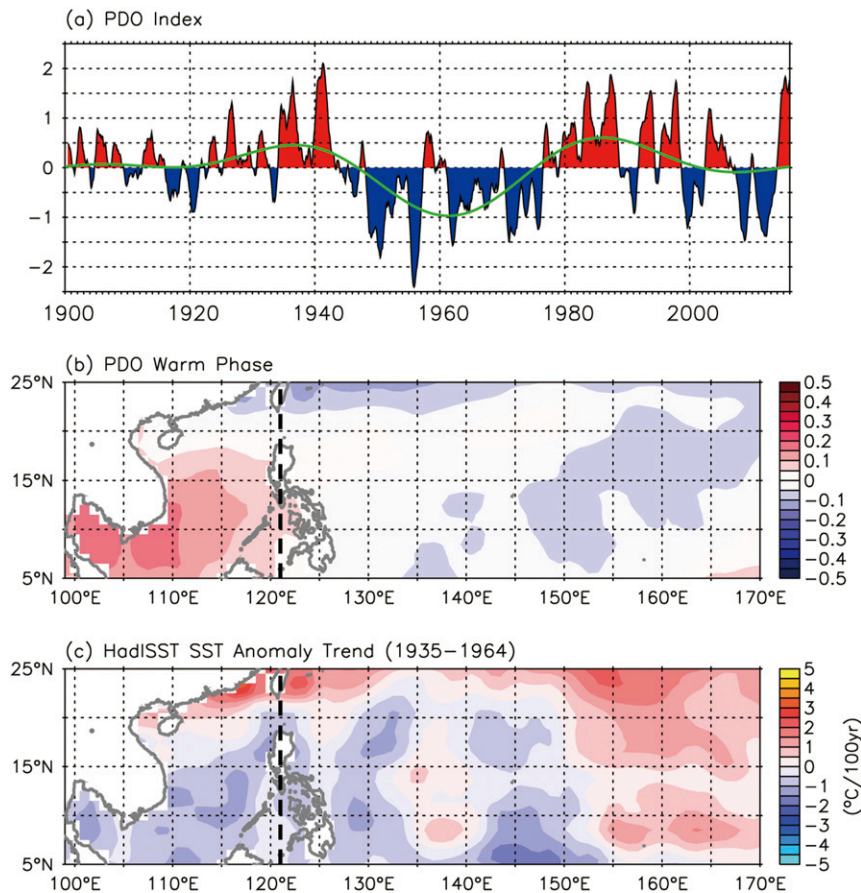


FIG. 9. (a) Time series of PDO index (HadISST) with a 1-yr moving average (red and blue) and 30-yr low-pass filter (green line) and (b) PDO warm phase. (c) Linear trend of the HadISST SST anomaly during 1935–64. Thick dashed line denotes the longitude of 121°E.

One may notice from the multidecadal tendency of temperature that larger warming rate occurred near the 26°–27°C isotherm. This is because the 26°–27°C isotherm is consistent with the top of the thermocline (or the bottom of the mixed layer) in the region. That is, a small vertical displacement of the isotherm could lead to a large change of temperature in the thermocline compared with that in the mixed layer. Besides, a warming (cooling) in the thermocline accompanies sinking (uplifting) of isotherms. By comparing the temperature in the first 15 years with the last 15 years during both three-decade periods, a stronger warming around the 26°–27°C isotherm occurred with a larger sinking of isotherms (black and green contours in Fig. 11). Furthermore, an uplifting of the 28°C isotherm took place for the surface cooling of temperature to the east of 150°E during 1960–89 (Fig. 11b). The outcome shows that a change in isotherms (involving the change of D26) in the whole water column above the D26 is the major controller for warming and cooling.

The temperature profile in the upper ocean could be influenced by several factors. The wind field is one of the most important factors, causing a vertical motion via the Ekman pumping that vertically transmits heat downward from the sea surface or upward from the subsurface. In addition, convergence and divergence induced by the horizontal velocity shear could be the other governing factors. As shown by contours in Fig. 11, the larger displacement of isotherms usually appears near the peak or trough of an isotherm, where it is usually associated with the divergent or convergent zone of two zonally flowing currents. In the studied area (Fig. 12a), the divergent area (peak) in the south is located along the edge between the eastward-flowing NECC (solid contour) and the westward-flowing NEC (dashed contour). The change of the pair of the two currents could cause a change of the isotherms across them. The comparison of velocity profiles on the two currents shows an insignificant change of the current strength (black and green contours in Figs. 12b–e).

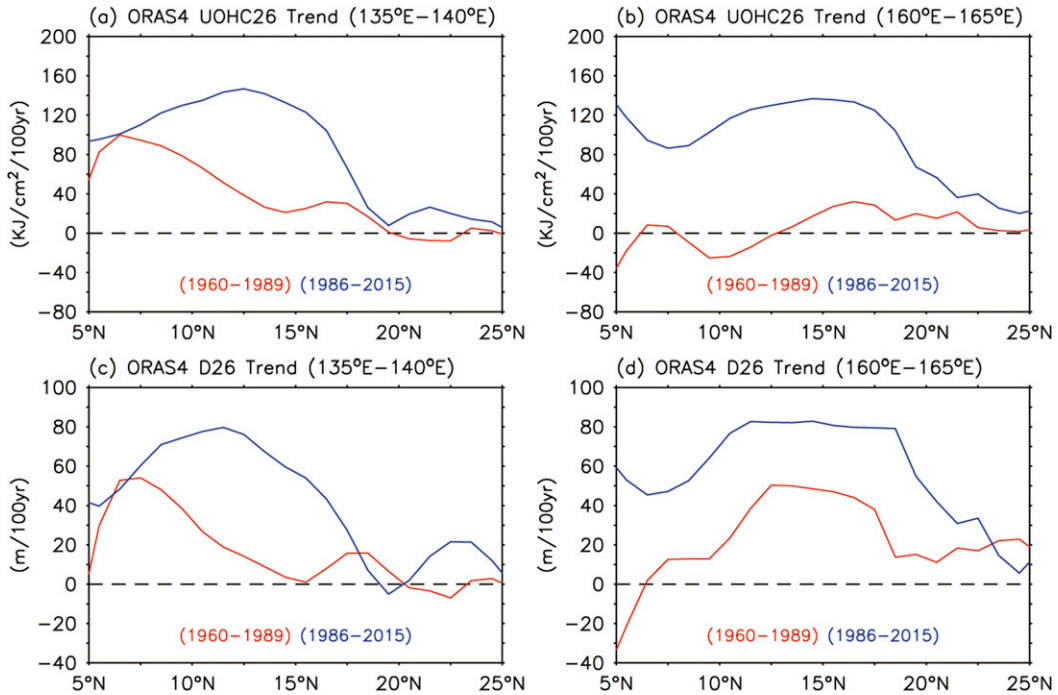


FIG. 10. Linear trends of the ORAS4 (top) UOHC26 and (bottom) D26 at (left) 135°–140°E and (right) 160°–165°E. Red and blue lines denote the trends during 1960–89 and 1986–2015, respectively.

Aside from the relative change of strength of two parallel currents, a horizontal shift of an individual current could accompany a horizontal shift of the underlying thermal structure, resulting in a change of

isotherms. For example, an isotherm below the mixed layer (say 26°C) across the NEC has a shallower depth in the south and a deeper depth in the middle. As the NEC migrates southward (Figs. 12b–e), the deeper

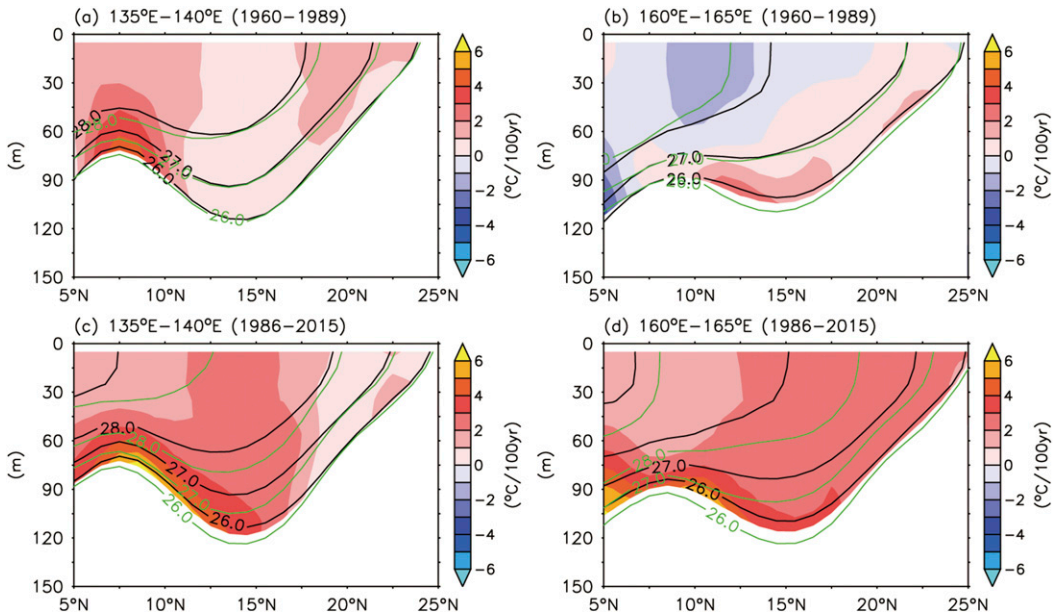


FIG. 11. Linear trends of the ORAS4 temperature of (left) 135°–140°E and (right) 160°–165°E during (top) 1960–89 and (bottom) 1986–2015 with mask (mean temperature <26°C). Black and green contours denote the ORAS4 temperature (>26°C) averaged over the earlier and later 15-yr period, respectively.

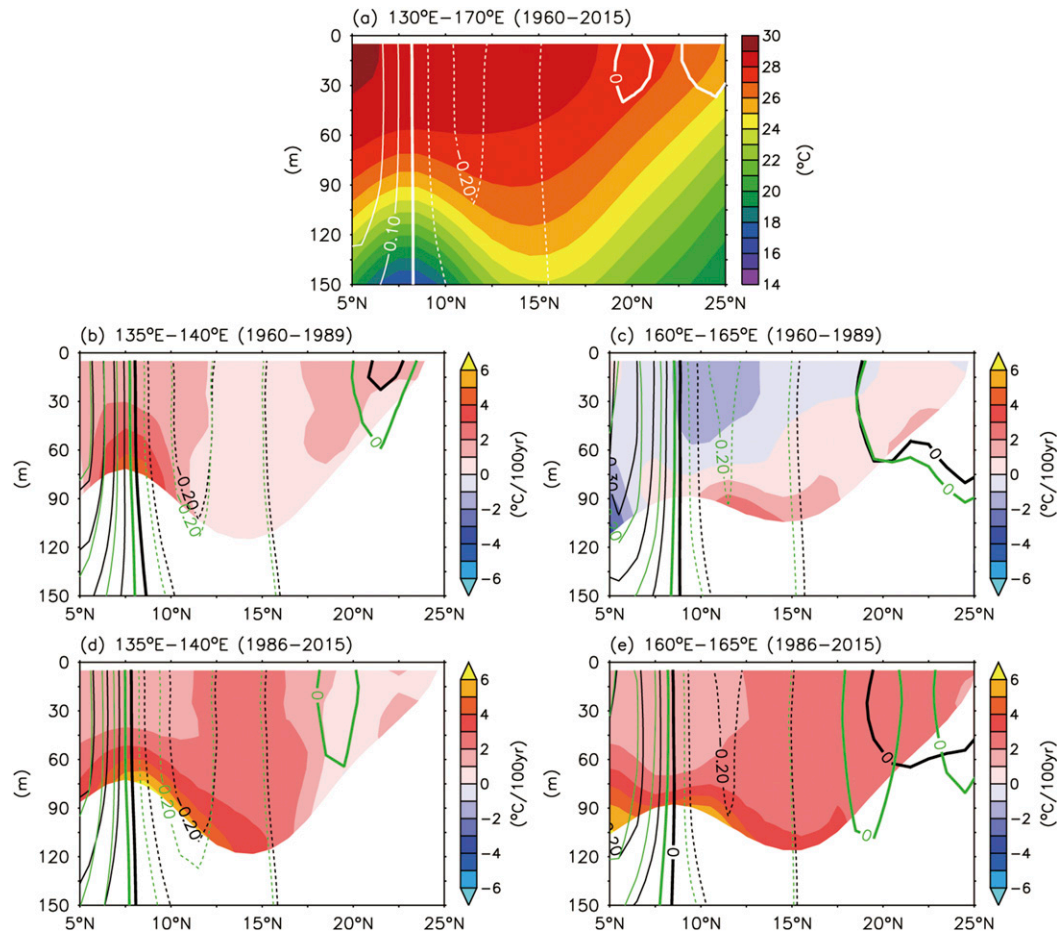


FIG. 12. (a) The ORAS4 temperature averaged over 130°–170°E from 1960 to 2015 with mean zonal velocity (white contour). (b)–(e) As in Figs. 11a–d, but black and green contours denote the ORAS4 zonal velocity averaged over the earlier and later 15-yr period, respectively.

isotherm in the middle shifts southward with depth unchanged, leading to a deepening of this isotherm in the south. One can conclude from the outcome that meridional movement of the NEC could be the major contributor to the vertical displacement of isotherms, leading to a strong subsurface warming around the top of the thermocline.

Similar vertical displacement of isotherms could be also found in the SCS. During 1960–1989 (Fig. 13a), warming and cooling trends took place in the surface and subsurface, respectively. After a transition in 1980s, warming occurred in the whole water column above the D26 during 1986–2015 (Fig. 13b). The warming in both periods seems to be transmitted from the sea surface. Besides, the SST in the SCS possessed an in-phase multidecadal change of warming trend (greater in the former three decades) with the temperature warming trends in the surface layer. The outcome indicates that the SST could be a major contributor to the UOHC26 in

the SCS. This fact may result from the shallower D26 in the SCS.

Aside from SST, the thermal structure in the SCS could be also determined by the basin-scale gyre circulation. Generally, the mean ocean circulation in the SCS is the cyclonic gyre with positive vorticity (e.g., Wyrтки 1961; Levitus 1984). As revealed in Figs. 13c and 13d, the basin-scale positive vorticity in 1960–89 intensified whereas the trends of vorticity in 1985–2015 became insignificant. During 1960–89, the significantly strengthening of basin-scale positive vorticity, indicative of an intensification of the SCS gyre circulation, induced an upward motion and uplifted the isotherm, leading to the subsurface cooling in 5°–10°N. Further, the subsurface cooling offset the greater surface warming (Fig. 13a), resulting in a smaller accumulating rate of UOHC26. Based on the above analyses, one can conclude that the multidecadal change of SST in the SCS can be

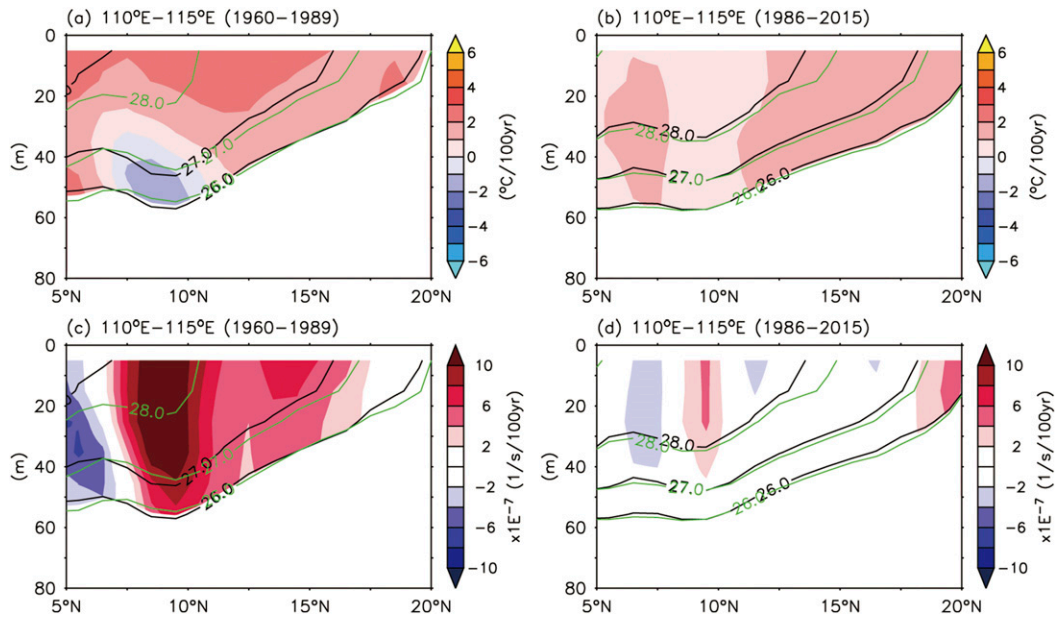


FIG. 13. Linear trends of the ORAS4 temperature of 110°–120°E during (a) 1960–89 and (b) 1986–2015 with mask (mean temperature <26°C). (c),(d) As in (a),(b), but for the linear trend of ORAS4 vorticity. Black and green contours denote the ORAS4 temperature (>26°C) averaged over the earlier and later 15-yr period, respectively.

connected to the PDO-related SST variability, while multidecadal change of ocean heat content is regulated by both the surface temperature and basin-scale ocean circulation.

5. Discussion and conclusions

The study utilizes the HadISST dataset and ORAS4 oceanic reanalysis product during 1960–2015 to investigate the multidecadal changes in surface and subsurface ocean conditions in the NWP region, including the TNWP and SCS. The analysis reveals that there was a transition in 1980s during the analyzed period of 1960–2015 for both the surface and subsurface environment in the TNWP and SCS. The 30-yr trends of SST and UOHC26 in the SCS and TNWP (including TNWPw and TNWPe) during 1960–89 and 1986–2015, and the possible factors resulting in the multidecadal changes of surface and subsurface conditions, are summarized in Fig. 14. In the SCS, the SST and UOHC26 had a similar evolution of warming tendencies, in which the warming is greater in the first three decades (top panel in Fig. 14). The multidecadal changes of oceanic thermal conditions in the TNWP differ, with divergent conditions in the TNWPw and TNWPe, where $\sim 150^\circ\text{E}$ is the dividing line. The SST warming trend in the TNWPw has a similar multidecadal change as that in the SCS, greater in the former three decades, but the UOHC26 experienced a greater warming in the latter

three decades. A totally different multidecadal change is found in the TNWPe. Cooling occurred in the former 30 years and SST warmed up afterward. An insignificant trend of UOHC26 is found in the first 30 years, and a huge accumulating rate of oceanic heat shows up in the last 30 years. Besides, we found that the accumulating UOHC26 is mainly contributed from the subsurface warming of temperature around the top of thermocline (or the bottom of mixed layer).

At the sea surface, the temperature trend in the whole NWP is associated with the PDO. The PDO-related SST trend shows an opposite pattern between the east and west of 150°E . As to the subsurface environment, changes of SST and subsurface isotherms take part in the multidecadal change of UOHC26. In the SCS, the UOHC26 is primarily dominated by the SST and secondarily by the isothermal variability due to the change of basin-scale gyre. In contrast, the change of isotherms plays a major role in generating a subsurface warming around the top of thermocline, and the PDO-related SST plays a minor role in the TNWP. The change of isotherms is ascribed to the southward shift of the NEC in terms of the multidecadal time scale. Based on the outcome in this study, it is worth noting that the change of upper-ocean circulation has to be taken into account in addressing the change of subsurface oceanic environment.

Besides, the results in the present study show that upper oceanic thermal conditions in the past six decades

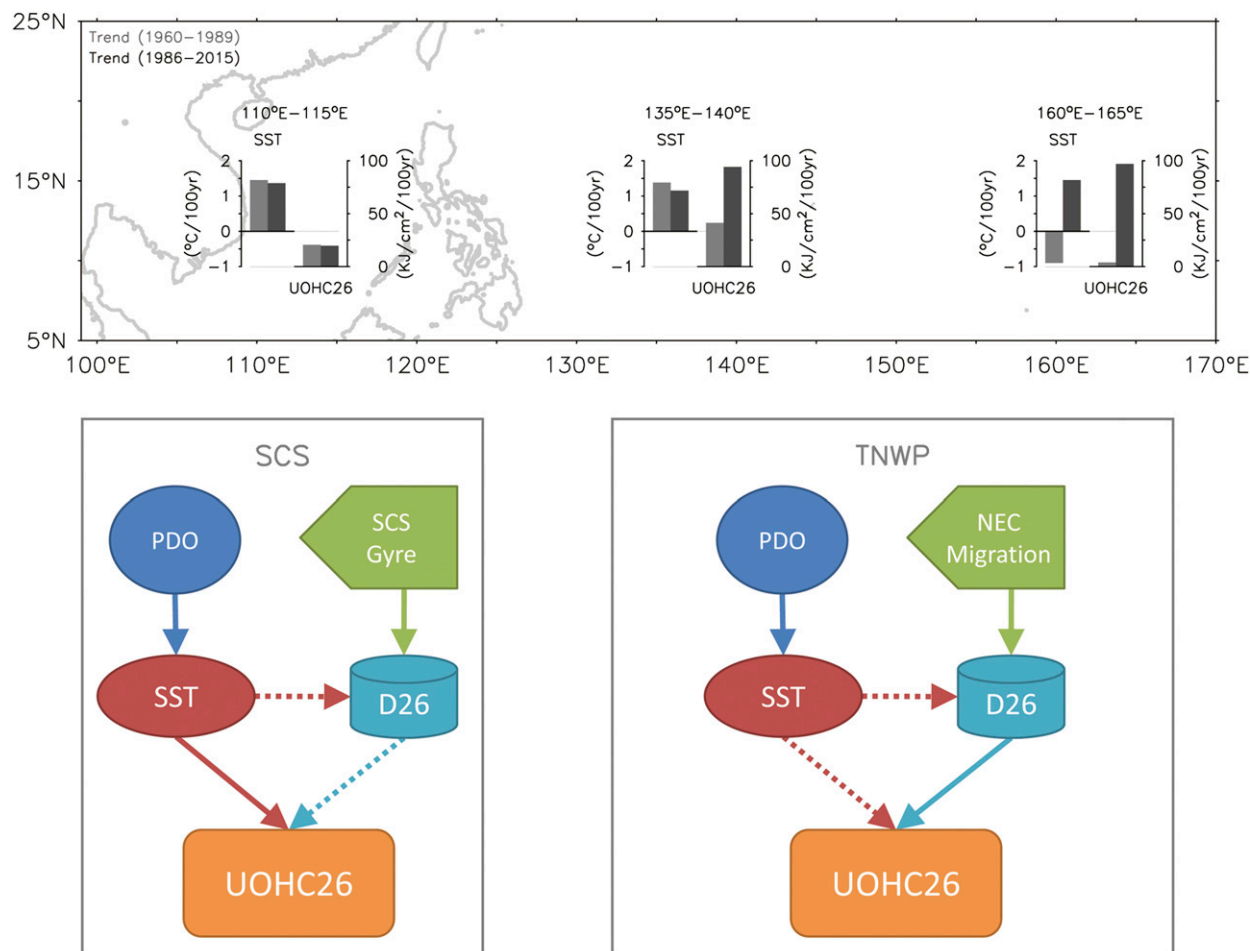


FIG. 14. (top) Linear trends (10° – 20° N) of the ORAS4 SST and UOHC26 of 110° – 115° E (SCS), 135° – 140° E (TNWPw), and 160° – 165° E (TNWPe) during 1960–89 (light gray bars) and 1986–2015 (dark gray bars). (bottom) Schematic diagram of possible factors resulting in the multidecadal changes of surface and subsurface thermal conditions in the SCS and TNWP.

could provide a favorable condition for the TC intensification in the NWP (TNWP and SCS). However, greater trends of UOHC26 were found in the latter three decades (~ 3 times greater compared to the first three decades) in the TNWP region, implying that much more energy supply in the TNWP might be available in this period, which may cause TCs to be more intensified. Normalized by the total amount of a year, trends of number of TC with maximum sustained wind speed (V_{max}) greater than 86.8 kt (the average V_{max} in the TNWP over 1960–2015; $1 \text{ kt} = 0.51 \text{ m s}^{-1}$) are further estimated for both three-decade periods based on the TC best-track data from the Joint Typhoon Warning Center. The outcome shows that the increasing trend in the latter period ($0.17\% \text{ yr}^{-1}$) was greater than that in the latter period ($0.01\% \text{ yr}^{-1}$), indicating that there are more and more intensified TCs occurring in the TNWP area in the latter three decades.

Acknowledgments. This research was supported by Taiwan Ministry of Science and Technology through Grants 105-2811-M-003-031, 106-2811-M-003-027, 104-2611-M-003-002-MY3, 105-2611-M-001-005, and 106-2611-M-001-007. The authors are grateful to the Ocean Climate Laboratory, National Centers for Environmental Information, National Oceanic and Atmospheric Administration, and Hadley Centre Met Office for the observation-based hydrographic data, the Asia-Pacific Data Research Center of International Pacific Research Center for the gridded Argo data, the European Centre for Medium-Range Weather Forecasts, the Predictive Ocean Atmosphere Model for Australia, and the Integrated Climate Data Center/Center for Earth System Research and Sustainability for the oceanic reanalysis products, and the Joint Typhoon Warning Center for the best-track data of tropical cyclone.

REFERENCES

- Balmaseda, M. A., K. Mogensen, and A. T. Weaver, 2013: Evaluation of the ECMWF ocean reanalysis system ORAS4. *Quart. J. Roy. Meteor. Soc.*, **139**, 1132–1161, <https://doi.org/10.1002/qj.2063>.
- Belkin, I. M., 2009: Rapid warming of large marine ecosystems. *Prog. Oceanogr.*, **81**, 207–213, <https://doi.org/10.1016/j.pocean.2009.04.011>.
- Bindoff, N. L., and Coauthors, 2007: Observations: Oceanic climate change and sea level. *Climate Change 2007: The Physical Science Basis*, S. Solomon et al. Eds., Cambridge University Press, 385–432.
- Chan, J. C., and K. S. Liu, 2004: Global warming and western North Pacific typhoon activity from an observational perspective. *J. Climate*, **17**, 4590–4602, <https://doi.org/10.1175/3240.1>.
- Chen, C.-T. A., and M.-H. Huang, 1996: A mid-depth front separating the South China Sea water and the Philippine Sea water. *J. Oceanogr.*, **52**, 17–25, <https://doi.org/10.1007/BF02236530>.
- Chiang, T.-L., C.-R. Wu, and L.-Y. Oey, 2011: Typhoon Kai-Tak: An ocean's perfect storm. *J. Phys. Oceanogr.*, **41**, 221–233, <https://doi.org/10.1175/2010JPO4518.1>.
- Emanuel, K. A., 1999: Thermodynamic control of hurricane intensity. *Nature*, **401**, 665–669, <https://doi.org/10.1038/44326>.
- Goni, G., and Coauthors, 2009: Applications of satellite-derived ocean measurements to tropical cyclone intensity forecasting. *Oceanography*, **22**, 190–197, <https://doi.org/10.5670/oceanog.2009.78>.
- Han, G., and W. Huang, 2008: Pacific decadal oscillation and sea level variability in the Bohai, Yellow, and East China Seas. *J. Phys. Oceanogr.*, **38**, 2772–2783, <https://doi.org/10.1175/2008JPO3885.1>.
- Hsin, Y.-C., 2016: Trends of the pathways and intensities of surface Equatorial Current System in the North Pacific Ocean. *J. Climate*, **29**, 6693–6710, <https://doi.org/10.1175/JCLI-D-15-0850.1>.
- Huang, P., I.-I. Lin, C. Chou, and R.-H. Huang, 2015: Change in ocean subsurface environment to suppress tropical cyclone intensification under global warming. *Nat. Commun.*, **6**, 7188, <https://doi.org/10.1038/ncomms8188>.
- Jin, F.-F., 1997: An equatorial ocean recharge paradigm for ENSO. Part I: Conceptual model. *J. Atmos. Sci.*, **54**, 811–829, [https://doi.org/10.1175/1520-0469\(1997\)054<0811:AEORPF>2.0.CO;2](https://doi.org/10.1175/1520-0469(1997)054<0811:AEORPF>2.0.CO;2).
- Köhl, A., 2015: Evaluation of the GECCO2 ocean synthesis: Transports of volume, heat and freshwater in the Atlantic. *Quart. J. Roy. Meteor. Soc.*, **141**, 166–181, <https://doi.org/10.1002/qj.2347>.
- Leipper, D. F., and D. Volgenau, 1972: Hurricane heat potential of the Gulf of Mexico. *J. Phys. Oceanogr.*, **2**, 218–224, [https://doi.org/10.1175/1520-0485\(1972\)002<0218:HHPOTG>2.0.CO;2](https://doi.org/10.1175/1520-0485(1972)002<0218:HHPOTG>2.0.CO;2).
- Levitus, S., 1984: Annual cycle of temperature and heat storage in the World Ocean. *J. Phys. Oceanogr.*, **14**, 727–746, [https://doi.org/10.1175/1520-0485\(1984\)014<0727:ACOTAH>2.0.CO;2](https://doi.org/10.1175/1520-0485(1984)014<0727:ACOTAH>2.0.CO;2).
- Lin, I.-I., C.-C. Wu, I.-F. Pan, and D.-S. Ko, 2008: Upper-ocean thermal structure and the western North Pacific category 5 typhoons. Part I: Ocean features and the category 5 typhoon's intensification. *Mon. Wea. Rev.*, **136**, 3288–3306, <https://doi.org/10.1175/2008MWR2277.1>.
- Locarnini, R. A., and Coauthors, 2013: *Temperature*. Vol. 1, *World Ocean Atlas 2013*, S. Levitus, Ed., NOAA Atlas NESDIS 73, 40 pp.
- Mantua, N. J., S. R. Hare, Y. Zhang, J. M. Wallace, and R. C. Francis, 1997: A Pacific interdecadal climate oscillation with impacts on salmon production. *Bull. Amer. Meteor. Soc.*, **78**, 1069–1079, [https://doi.org/10.1175/1520-0477\(1997\)078<1069:APICOW>2.0.CO;2](https://doi.org/10.1175/1520-0477(1997)078<1069:APICOW>2.0.CO;2).
- Mei, W., C.-C. Lien, I.-I. Lin, and S.-P. Xie, 2015: Tropical cyclone-induced ocean response: A comparative study of the South China Sea and tropical northwest Pacific. *J. Climate*, **28**, 5952–5968, <https://doi.org/10.1175/JCLI-D-14-00651.1>.
- Newman, M., and Coauthors, 2016: The Pacific decadal oscillation, revisited. *J. Climate*, **29**, 4399–4427, <https://doi.org/10.1175/JCLI-D-15-0508.1>.
- Peduzzi, P., B. Chatenoux, H. Dao, A. De Bono, C. Herold, J. Kossin, F. Mouton, and O. Nordbeck, 2012: Global trends in tropical cyclone risk. *Nat. Climate Change*, **2**, 289–294, <https://doi.org/10.1038/nclimate1410>.
- Price, J. F., 1981: Upper ocean response to a hurricane. *J. Phys. Oceanogr.*, **11**, 153–175, [https://doi.org/10.1175/1520-0485\(1981\)011<0153:UORTAH>2.0.CO;2](https://doi.org/10.1175/1520-0485(1981)011<0153:UORTAH>2.0.CO;2).
- Pun, I.-F., I.-I. Lin, C.-R. Wu, D.-S. Ko, and W.-T. Liu, 2007: Validation and application of altimetry-derived upper ocean thermal structure in the western North Pacific Ocean for typhoon-intensity forecast. *IEEE Trans. Geosci. Remote Sens.*, **45**, 1616–1630, <https://doi.org/10.1109/TGRS.2007.895950>.
- Qiu, B., 2003: Kuroshio Extension variability and forcing of the Pacific decadal oscillations: Responses and potential feedback. *J. Phys. Oceanogr.*, **33**, 2465–2482, <https://doi.org/10.1175/2459.1>.
- Rayner, N. A., D. E. Parker, E. B. Horton, C. K. Folland, L. V. Alexander, D. P. Rowell, E. C. Kent, and A. Kaplan, 2003: Global analyses of sea surface temperature, sea ice, and night marine air temperature since the late nineteenth century. *J. Geophys. Res.*, **108**, 4407, <https://doi.org/10.1029/2002JD002670>.
- Stocker, T. F., and A. Schmittner, 1997: Influence of CO₂ emission rates on the stability of the thermohaline circulation. *Nature*, **388**, 862–865, <https://doi.org/10.1038/42224>.
- Thompson, B., P. Tkalich, and P. Malanotte-Rizzoli, 2017: Regime shift of the South China Sea SST in the late 1990s. *Climate Dyn.*, **48**, 1873–1882, <https://doi.org/10.1007/s00382-016-3178-4>.
- Trenberth, K. E., and Coauthors, 2007: Observations: Surface and atmospheric climate change. *Climate Change 2007: The Physical Science Basis*, S. Solomon et al., Eds., Cambridge University Press, 235–336.
- Wallace, J. M., E. M. Rasmusson, T. P. Mitchell, V. E. Koussy, E. S. Sarachik, and H. von Storch, 1998: On the structure and evolution of ENSO-related climate variability in the tropical Pacific: Lessons from TOGA. *J. Geophys. Res.*, **103**, 14 241–14 259, <https://doi.org/10.1029/97JC02905>.
- Wu, C.-C., C.-Y. Lee, and I.-I. Lin, 2007: The effect of the ocean eddy on tropical cyclone intensity. *J. Atmos. Sci.*, **64**, 3562–3578, <https://doi.org/10.1175/JAS4051.1>.
- Wu, C.-R., 2013: Interannual modulation of the Pacific decadal oscillation (PDO) on the low-latitude western North Pacific. *Prog. Oceanogr.*, **110**, 49–58, <https://doi.org/10.1016/j.pocean.2012.12.001>.
- , Y.-L. Wang, Y.-F. Lin, T.-L. Chiang, and C.-C. Wu, 2016: Weakening of the Kuroshio intrusion into the South China Sea under the global warming hiatus. *IEEE J. Sel. Top. Appl. Earth Obs. Remote Sens.*, **9**, 5064–5070, <https://doi.org/10.1109/JSTARS.2016.2574941>.
- Wu, L., and Coauthors, 2012: Enhanced warming over the global subtropical western boundary currents. *Nat. Climate Change*, **2**, 161–166, <https://doi.org/10.1038/nclimate1353>.

- Wyrski, K., 1961: *Physical Oceanography of the Southeast Asian Waters*. Vol. 2, *Scientific Results of Marine Investigation of the South China Sea and the Gulf of Thailand*. Scripps Institution of Oceanography, 195 pp.
- Yin, Y., O. Alves, and P. R. Oke, 2011: An ensemble ocean data assimilation system for seasonal prediction. *Mon. Wea. Rev.*, **139**, 786–808, <https://doi.org/10.1175/2010MWR3419.1>.
- Yu, J.-Y., M.-M. Lu, and S. T. Ki, 2012: A change in the relationship between tropical central Pacific SST variability and the extratropical atmosphere around 1990. *Environ. Res. Lett.*, **7**, 034025, <https://doi.org/10.1088/1748-9326/7/3/034025>.
- Zheng, Z.-W., I.-I. Lin, B. Wang, H.-C. Huang, and C.-H. Chen, 2015: A long neglected damper in the El Niño–typhoon relationship: A ‘Gaia-like’ process. *Sci. Rep.*, **5**, 11103, <https://doi.org/10.1038/srep11103>.